De-icing of overhead cables by mechanical shocks: numerical and experimental analyses

T. Kálmán and M. Farzaneh

NSERC / Hydro-Québec / UQAC Industrial Chair on Atmospheric Icing of Power Network Equipment (CIGELE) and Canada Research Chair on Engineering of Power Network Atmospheric Icing (INGIVRE) at Université du Québec à Chicoutimi, Québec, Canada, G7H 2B1
t.kalman@freemail.hu and mfarzaneh@uqac.ca

G. McClure

Department of Civil Engineering and Applied Mechanics, McGill University, Montréal, Canada, H3A 2K6
ghyslaine.mcclure@mcgill.ca

A. Leblond

Hydro-Québec TransÉnergie, Montréal, Canada, H2L 4M8
leblond.andre.2@hydro.qc.ca

Abstract—**A numerical model that explicitly considers the rupture of the ice deposit by including the mechanical properties of ice into the model is proposed. This model calculates the dynamic effects of ice shedding induced by an external shock load on a single-span overhead line section. The model can serve as a basis to study various failure criteria of atmospheric glaze ice in terms of axial and bending stress-strain relations and strain-rate effects, in particular. A comparison of numerical and experimental results of a level single-span reduced-scale experimental model is presented in an attempt to validate the numerical model.**

I. INTRODUCTION

IN cold regions, overhead line cables and their supporting structures are usually exposed to atmospheric icing. In addition, global climate warming is expected to increase the risks associated with extreme weather events which in turn could possibly increase the frequency and severity of storms such as winter blizzards and freezing rain storms [1].

Several types of atmospheric icing deposits may load overhead cables including heavy adherent wet snow, hard rime, large but lightweight rime ice, and dense glaze ice [2]. Ice deposits on exposed structures can be the source of several mechanical problems. On overhead power lines in particular, the gravity loads due to heavy ice accretion, coupled with wind-on-ice loads, may lead to structural damages or failure and even cascading collapse of towers [2]. Therefore, in order to protect the line against loads resulting from accreted ice and to ensure the reliability of electrical power delivery networks, various mitigation methods have been used. A de-icing technique of interest, in this study, uses mechanical impulses to de-ice ground wires by taking advantage of the brittle behavior of ice at high strain rates [3].

This study therefore focuses on the dynamic analysis of iced overhead transmission lines subjected to in-span shock loads. Such in-span loads may result from the effect of an external shock load intended to remove accreted ice from the cable or from load imbalances due to sudden ice shedding. In particular, the dynamic response of iced cables under shock loads is studied by numerical modeling using nonlinear finite element analysis. The objective is to understand the phenomenon of mechanically-induced ice shedding on overhead line sections. Numerical studies of ice shedding on lines are scarce, and in most previous work [4-6], the response of the line to instantaneous shedding was modeled, whereas in this research, the propagation of ice shedding along the span as an "unzipping" effect is studied.

II. NUMERICAL MODEL ELABORATION

In previous work [9, 10], the authors have presented a novel approach to model the failure propagation of the ice deposit along the span by developing a special iced cable finite element that integrates the failure criteria of the ice deposit. In this section, the general numerical modeling approach originally proposed in [8] for transient analysis of overhead transmission lines using ADINA [12], and enriched in the last decades by collaborators [5-7], including our recent contributions, is summarized.

A. Cable modeling

The cable is assumed to be perfectly flexible in bending and torsion; therefore it is represented by 3-D two-node isoparametric truss elements using the total Lagrangian formulation with large displacement kinematics but small strains [12, 13]. The cable material properties are linear elastic tension-only, therefore allowing slackening whenever the cable loses its pre-stressing force. The cable mesh density is selected to provide adequate sampling of the shock propagation through the integration points of the model.

B. Accreted ice modeling

Accreted ice on the cable is modeled as a separate beam element parallel to each cable element (Fig. 1). Each beam element has six degrees-of-freedom corresponding to the horizontal and vertical translations and the in-plane rotation. In order to avoid spurious stiffening of the system caused by fixed rotational boundary conditions at the supports, ice beam elements are omitted just next to the support nodes. It was found adequate to represent the accreted ice on the cable either by the 3-D iso-beam, the 2-D plane stress iso-beam or the pipe-beam elements with inelastic behavior.

For the materially nonlinear iso-beam elements in ADINA, only rectangular cross sections can be considered, while this geometrical restriction does not apply to the pipe-beam element [12]. The use of the 2-D plane stress iso-beam ice model reduces the computational effort considerably, which may be important when complex models are used. However, numerical simulations [10, 11] showed that it may result in shear locking [13]. On the other hand, the 3-D iso-beam yields results that are very consistent with those obtained with the pipe-beam ice model, and in this study, the 3-D iso-beam element is finally selected to represent the accreted ice on the cable.
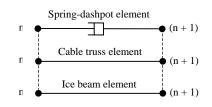

Fig. 1. Iced cable model representation (n – nodes)

C. Ice failure modeling

The failure criteria of glaze ice in terms of axial and bending stress-strain relations, and strain rate effects are based on the mechanical properties of fine-grained freshwater ice published in the literature, since it is the best information available [11]. However, further refinements of the failure criteria of glaze ice deposits can be readily integrated into this model as they become available.

Ice failure and subsequent shedding or detachment is modeled using the *"element death upon rupture"* option available in ADINA. For the beam ice elements used with the plastic bilinear material model, the element death option is automatically activated when the rupture criterion is fulfilled at any given integration point of the element. The ice material model is defined in ADINA by setting the Young's modulus to 10 GPa, the Poisson's ratio to 0.3, the density to 900 kg/m^3, the initial yield stress to 2 MPa, and the maximum allowable effective plastic strain to 10^{-10}.

D. Damping

In this work, based on satisfactory results of previous studies [5-8], the aerodynamic damping is neglected and only axial structural damping of the cable is considered. Therefore,

damping is modeled by using a non-linear axial spring element as a viscous discrete dashpot parallel to each cable element (Fig. 1). Besides this viscous structural damping, algorithmic (numerical) damping is also used to filter out spurious high frequencies of the response due to finite element discretization [9-11].

E. Other considerations

The deformed iced cable profile is calculated beforehand using an increased density cable model as in previous studies [5-7]. This deflected static profile serves as the initial profile of the ice-cable composite model where the cable element is assigned the value of initial strain obtained from static analysis of the increased density cable model. Dynamic analysis is started from the static equilibrium profile obtained for the composite model. The Newmark direct implicit integration method is selected to solve the dynamic equilibrium equations, with the full Newton iteration method for stiffness updates. A lumped mass formulation is used throughout [12, 13].

III. EXPERIMENTAL STUDY

Experimental validation of ice shedding problems at the real scale is still incomplete as such tests are difficult and costly to achieve. Therefore, considering the lack of availability of a real-scale test line, a level single-span reduced-scale experimental model is proposed in an attempt to validate the numerical model. Despite that no direct correlation can be made between reduced-scale and real-scale lines due to high nonlinearities of the problem and the exaggerated sensitivities of the reduced-scale model, it is believed that the reduced-scale model can serve to analyze and better understand the problem. It is also believed that if the numerical results of the level single-span reduced-scale experimental model agree with those obtained experimentally, the modeling approach can be used for simulations of real-scale lines as well.

A. Experimental setup

The experimental setup is installed at the CIGELE icing precipitation simulation laboratory. This laboratory is equipped with a water spraying unit and housed in a refrigerated room where the air temperature is controlled and can reach -20 ℃ [11]. The setup installed in front of the water spraying unit (Fig. 2) consists of two rigid supports mounting a flexible stainless steel cable (RR-W-410D) pin-ended to load cells using hinged arms (Fig. 3a). The length of the cable is defined to provide an initial sag-to-span ratio of 6% with a span length of 4 m. The shock load (impact) is provided by a pneumatic cylinder (Parker series 2A) (pneumatic shock load generator) installed at the cable mid span, which is part of a pneumatic system [11]. Horizontal and vertical components of the cable end-tensions are measured using low profile universal pancake load cells manufactured by FUTEK (model: LCF 450 – 500 lbf). The bridge excitation for each load cell is provided by a signal conditioner amplifier manufactured also by FUTEK (model: CSG110). The shock load is measured by

an ICP® low-impedance quartz force sensor manufactured by PCB Piezotronics Inc. (model: N223M11 – 250 lbf). The force sensor is mounted on the tip of the pneumatic cylinder piston rod (Fig. 3b). Power to operate the sensor is provided by a signal conditioner manufactured also by PCB Piezotronics Inc. (model: 482A22). Analog to digital conversion is provided by a USB function module manufactured by Data Translation Inc. (model: DT9804). A measurement application is built using a commercial test and measurement application software called DT Measure Foundry [14]. A high speed digital camera manufactured by Kodak (model: EktaPro 1012) is used to capture the cable mid-span displacement.
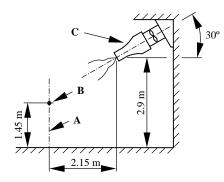

Fig. 2. Schematic transverse view of the level single-span reduced-scale experimental setup and the water spraying unit configuration (A: center line of the setup; B: approximate cable height at mid span; C: water spraying unit)
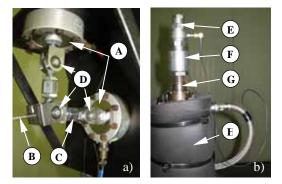

Fig. 3. a) Pin-ended stainless steel cable end connection; b) ICP® force sensor installation (A: load cells; B: stainless steel cable; C: hinged arm; D: ball bearings; E: ICP® force sensor; F: mounting stud; G: piston rod; H: insulator covered air cylinder)

B. Description of a typical test

A typical test sequence comprises four major steps: (1) producing a glaze deposit on the cable; (2) applying a shock load to the iced cable by actuating the shock load generator; (3) measuring and recording the characteristics of the shock load, the generated dynamic cable end-tensions and the cable mid-span displacement; and the (4) data processing. Experimental parameters that define the type and properties of ice in the icing precipitation laboratory [11] are controlled in order to obtain a glaze deposit with a density close to 900 kg/m³ and to reduce the time needed for the ice formation.

IV. COMPARISON OF NUMERICAL AND EXPERIMENTAL RESULTS

Several icing scenarios were studied that comprise bare and iced cable models with 1, 2 and 4 mm of equivalent radial ice thickness [11]. However, in this paper, only results of the bare and an iced cable models with 4 mm of equivalent radial ice thickness are presented. The numerical and experimental results of the bare line subjected to a shock load are compared first in order to assess the parameters of the numerical model. A stainless steel cable with a diameter of 4.1 mm is used throughout the analyses.

A. Bare cable model

In the experimental setup, the cable and the centers of the attachment points at the end of the span are aligned so that the cable is in the same plane along its entire length. Furthermore, the shock loading piston setup at the mid span is also aligned in the cable plane. Therefore, the numerical model is also represented in the same 2-D plane. At this stage of analysis, the flexibility of the supports is not modeled and the cable ends are assumed to be rigidly fixed. The cable material model is linear elastic tension-only with a constant axial rigidity (EA) of 2,275,680 N (MAT-1). In the model used here, the length of each cable element is found to be adequate by using a mesh of 25 elements, i.e. each element has a length of about 0.16 m with a constant cross-sectional area of 13.2 mm². The damping constant is set to represent an equivalent viscous damping of 2% critical. A value smaller than the one (3-5%) observed in an investigation based on free vibration measurements [11] is chosen because some numerical damping is also introduced as indicated in Section II. In order to provide adequate sampling of the shock wave as it travels through the cable finite element mesh, the time step is set to 0.25 ms considering also the sampling rate of each parameter measured during the experiments. Several experimental tests were performed on the bare cable model at ambient temperature to investigate the nature of the problem and to obtain several data sets for comparison purposes. In this paper, comparisons of the numerical and experimental results of only one test with a measured shock load (Fig. 4) are presented. This shock load function serves as an input to the numerical model and is applied to the cable at mid span in the vertical upward direction.

Figures 5a and b present comparisons between the time history of cable tension calculated by the numerical model and that obtained experimentally after the shock load of Fig. 4 was applied to the cable at t = 1.05 s. All values before t = 1.05 s represent the static response of the system subjected to its self-weight. The static initial tension of the cable is 5.86 N. It is seen that the most severe dynamic effect occurs during the
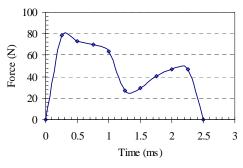
Fig. 4. Shock load characteristics

first second following the shock load. Comparison of the time history of the cable tensions (Fig. 5a) shows general agreement between the calculated and measured values. However, the first peak value of cable tension obtained numerically is overestimated compared to that obtained experimentally (Fig. 5b). Comparisons of other results of this test series show the same discrepancy, i.e. the first peak value of cable tension obtained numerically is overestimated while the rest of the graph shows good agreement between the measured and calculated values. The problem is assumed to arise from the sensitivity of the numerical model to the flexibility of the cable end supports of the experimental setup, which is not considered in the numerical model at this stage of analysis, and also from the simplifying assumption in modeling the tensional rigidity of the cable. Comparisons of the time history of the cable mid-span displacements (Fig. 5c) reveal that the maximum cable jump at the mid span is accurately calculated by the numerical model. However, amplitude decay can be observed for the second and third peaks of the cable jump while there is agreement on the time scale. Zero displacement refers to the bare cable initial state.

In order to study the sensitivity of the reduced-scale numerical model, a number of parametric studies were performed introducing support flexibility and a more realistic cable extension material model [11]. Support flexibility in the numerical model is introduced by modeling the hinged support arms with linear spring elements with arbitrary axial rigidity values. The more realistic cable extension material model is defined as a linear approximation of the experimental stress-strain curve of the cable in the region of prevailing loads. The cable was characterized using standard static tensile tests in accordance with ASTM A 931-96 (2002) [15].

Sensitivity studies of the numerical model reveal that the most accurate predictions of the maximum cable tension are obtained when the effects of system flexibility that may arise from either the end supports or the cable itself are taken into account [11]. Both improvements tend to yield accurate results for the maximum cable tension: the more flexible the support is, the smaller the amplitude of the maximum cable tension, which shows convergence towards the experimental value. However, the results obtained for the maximum cable jump at mid span
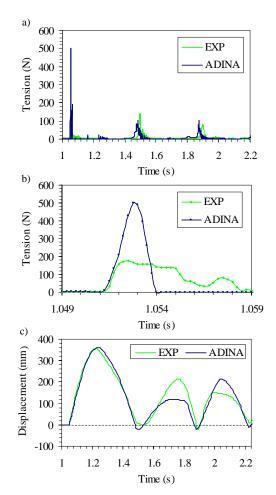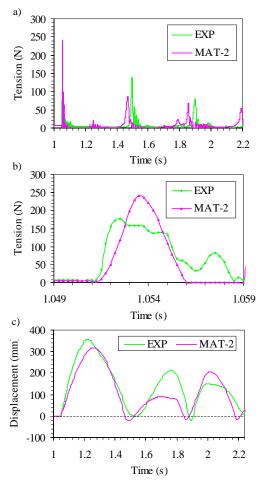

Fig. 5. Comparison of numerical and experimental results of cable tension at the support and mid-span displacement: a) time history of cable tension; b) first peak of cable tension; c) vertical mid-span displacement

show the reverse tendency i.e. stiffer supports yield more accurate predictions of the maximum mid-span displacement. Moreover, the displacements of the cable attachment points obtained in the numerical simulations with flexible supports were not observed in the physical tests. Therefore, it is assumed that the effect of system flexibility of the reduced-scale experimental model derives essentially from the flexibility of the stainless steel cable used.

The use of the improved cable material (MAT-2) model results in a decrease of 52% of the maximum cable tension (c.f. Fig. 5b and Fig. 6b) without severe distortion of the time history results (Fig. 6a). However, a shift of the period can be observed compared to that obtained by the numerical model using the initial (MAT-1) taut cable modeling approach (c.f. Fig. 5 and Fig. 6). Furthermore, the predicted cable mid-span displacement is also more accurate with the latter material model (c.f. Fig. 5c and Fig. 6c). These reverse tendencies can be explained by the fact that the displacements and tensions are not measured at the same location, and that when the shock load is applied to the cable at the mid span, a transverse as well as a longitudinal wave is generated that induces the maximum cable tension at the support. However, the energy of the shock load is dissipated much faster in a flexible cable

(in both tensional and flexural effects) than in a taut cable before hitting the supports, resulting in a smaller value of peak cable tension at the support. Nevertheless, when the cable is in vertical motion, it behaves as a taut cable.

As a conclusion of these sensitivity studies, the 25-element numerical model is used in the remaining analysis of the iced cable using the taut cable material model (MAT-1 EA = 2,275,680 N) to generate the time history results of mid-span displacement, and the flexible cable material model (MAT-2 EA = 346,500 N) to obtain the time history results of cable tension at the support.

a)

b)

c)

Fig. 6. Comparison of numerical and experimental results of cable tension at the support and mid-span displacement using MAT-2 cable material model: a) time history of cable tension; b) first peak of cable tension; c) vertical mid-span displacement

B. Iced cable model

Despite the fact that the cable and the shock load applied at mid span are practically in the same plane, a small out-of-plane motion of the cable is observed during the experiments when the shock load is applied. Asymmetric ice accretion on the cable could not be avoided, which induced eccentric out-of-plane forces. Nevertheless, accreted ice on the cable is modeled as a separate 3-D two-node iso-beam element with rectangular cross-section parallel to each cable element in the 2-D plane, as described in Section II. The cross-sectional dimensions of the numerical ice-beam (W = 11.00 mm, H =

7.09 mm) [13] are specified to yield a bending stiffness equivalent to the idealized tubular shape of accreted ice. Due to limitations of the spraying trajectory, 30 cm of the cable at both ends of the span remained ice free. Therefore, two ice elements are omitted at both ends of the span just next to the support nodes and fixed rotational boundary conditions are assigned to nodes 2 and 25 (Fig. 7).
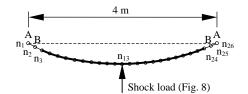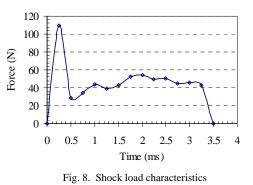
Fig. 7. Schematic of the reduced-scale numerical ice-cable composite model

Figure 8 shows the characteristics of shock load measured and defined as input to the numerical model for the ice-shedding scenario studied.

Fig. 8. Shock load characteristics

The time histories of Fig. 9 compare numerical and experimental results of cable tension and mid-span displacement, while Fig. 10 shows the rate of ice shedding in the span, i.e. the fraction of the ice shed in the span.

The maximum cable jump at the mid span is accurately computed by the numerical model (Fig. 9c) but the numerical model predicts higher jumps for the second and third peaks compared to the experimental model. This is linked to the fact that the effective rate of ice shedding calculated by the numerical model is higher than that obtained experimentally (Fig. 10).

In the experiments, effective ice shedding occurs at the mid span where the shock load is applied, on a length of about 25 cm, as well as at a distance of about 37 cm from the point of impact in the two directions, on a length of only about 2 cm. However, a portion of the ice that remains attached to the cable is extensively cracked. This is due to the fact that the shock load applied at the mid span generates a transverse wave in the cable that (in contrast with real-scale lines [9-11]) quickly transforms into a longer vibrating loop with a wave length of about 74 cm that further expands to the whole span. Effective ice shedding takes place where the transverse wave propagation is directly observed and where the long vibrating loop forces the cable to bend significantly. Elsewhere

(highlighted in grey in Fig. 10) extensive cracking of the ice deposit is observed but shedding is not triggered due to the adhesive strength of ice on the cable, which is not considered in the numerical model. Therefore, when the failure criterion of the ice in terms of axial and bending stress-strain relations is fulfilled at any integration point, the ice element mass and stiffness contributions are removed from the model, i.e. effective ice-shedding is assumed to take place. Based on this failure criterion, comparisons of numerical and experimental results of ice shedding (Fig. 10) reveal that the rate and the location of the ice shedding are nonetheless satisfactorily calculated by the numerical model.
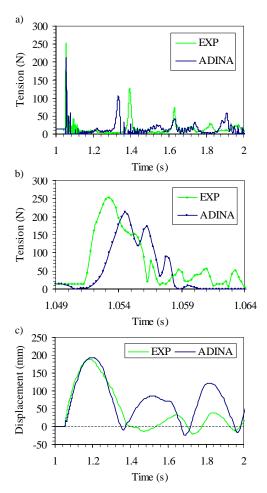

Fig. 9. Comparison of numerical and experimental results of cable tension at the support and mid-span displacement for the ice-shedding scenario studied: a) time history of cable tension; b) first peak of cable tension; c) vertical mid-span displacement
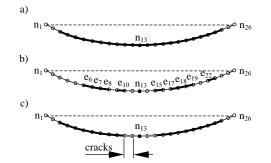

Fig. 10. Rate of ice shedding obtained by ADINA and experiments for the ice-shedding scenario studied: a) iced cable before the shock load; b) cable after the shock load by ADINA; c) cable after the shock load by experiments

V. CONCLUSIONS

Comparisons of numerical and experimental results indicate that the numerical model accurately calculates the dynamic response of iced cables subjected to shock loads. However, the reduced-scale model is highly sensitive to cable flexibility. Nevertheless, it is believed that no such degree of sensitivity characterizes a real-scale line. Furthermore, even if the numerical model does not consider the adhesive strength of ice deposit that appears to be important in the reduced-scale model, it seems that until the transverse wave and its propagation along the span is maintained, i.e. the ice deposit is subjected to a high level of bending, the occurrence of effective ice shedding from the cable is a reasonable assumption. This has been verified by numerical analysis of real-scale lines [9-11] and also in experimental studies performed by Hydro-Québec TransÉnergie on a 100-m test span of a ground wire [3]. Therefore, we conclude that the numerical model presented can accurately model the dynamic effects of shock-load-induced ice shedding on overhead lines when this transverse wave propagation is observed. However, experimental validation of the numerical model results on a real-scale line is paramount.

VI. ACKNOWLEDGMENT

VII. REFERENCES

[1] H. Hengeveld, B. Whitewood and A. Fergusson, "An introduction to climate change: A Canadian perspective", Canada: Minister of Public Works and Government Services, 2005.

[2] CIGRE Technical Brochure n° 291, "Guidelines for meteorological icing models, statistical methods and topographical effects", Working Group B2.16, Task Force 03, April 2006.

[3] A. Leblond, B. Lamarche, D. Bouchard, B. Panaroni and M. Hamel, "Development of a portable de-icing device for overhead ground wires", in Proc. 2005 11th International Workshop on Atmospheric Icing of Structures, pp. 399-404.

[4] M. Matsuura, H. Matsumoto, Y. Maeda and Y. Oota, "The study of ice shedding phenomena on transmission lines", in Proc. 1995 1st International Symposium on Cable Dynamics, pp. 181-188.

[5] A. Jamaleddine, G. McClure, J. Rousselet and R. Beauchemin, "Simulation of ice shedding on electrical transmission lines using ADINA", Computers and Structures, vol. 47 (4/5), pp. 523-536, 1993.

[6] M. Roshan Fekr and G. McClure, "Numerical modeling of the dynamic response of ice shedding on electrical transmission lines", Atmospheric Research, vol. 46, pp. 1-11, 1998.

[7]   G. McClure and M. Lapointe, "Modeling the structural dynamic response of overhead transmission lines", Computers and Structures, vol. 81, pp. 825-834, 2003.

[8]   G. McClure and R. Tinawi, "Mathematical modeling of the transient response of electric transmission lines due to conductor breakage", Computers and Structures, vol. 26 (1/2), pp. 41-56, 1987.

[9]   T. Kálmán, M. Farzaneh, G. McClure, L.E. Kollár and A. Leblond, "Dynamic behavior of iced overhead cables subjected to mechanical shocks", in Proc. 2005 6th International Symposium on Cable Dynamics, pp. 339-346.

[10] T. Kálmán, M. Farzaneh and G. McClure, "Numerical analysis of the dynamic effects of shock-load-induced ice shedding on overhead ground wires", Computers and Structures, vol. 85, pp. 375-384, 2007.

[11] T. Kálmán, "Dynamic behavior of iced cables subjected to mechanical shocks", Ph.D. Thesis, University of Québec at Chicoutimi, Canada, 2007.

[12] ADINA Theory and Modeling Guide, ADINA R&D Inc., Watertown, MA, USA, Sep. 2004.

[13] K.J. Bathe, "Finite element procedures", Upper Saddle River, NJ, USA: Prentice Hall, 1996.

[14] DT Measure Foundry, Data Translation Inc., Marlboro, MA, USA, 2005.

[15] A 931-96 (2002): Standard test method for tension testing of wire ropes and strand, 2004 Annual Book of ASTM Standards, Iron and Steel Products, vol. 01.03, pp. 489-493.